An Average Modeling Approach for Mobile Refrigeration Hybrid Power Systems with Improved Battery Simulation

Yue Cao, *Student Member*, *IEEE*, Philip T. Krein, *Fellow, IEEE*

***Abstract*—This paper presents averaging-based models of hybrid electric power systems for refrigeration units in delivery trucks. The model is intended to be used for a system-level power and energy flow study and eventually for a development of prototypes. Challenges unique to this hybrid application, including the thermal system interface, drive cycle response, and battery management, are introduced. The system topology is presented, including the hybrid power architecture, electrical-thermal system specifications, and the integrated model operation and controls. The modeling approach for each electrical component, including ac machines, the battery set, and converters, is discussed. An average modeling technique is used, because it can track system-level power and efficiency over a long time interval with fast simulation. Battery simulation is improved from previous literature to provide a more accurate and robust solution. The model, interfaced with the thermal system, is verified by simulation studies in MATLAB/Simulink. The average model is also validated through experiments, including an active front end test, a battery test, and a variable speed ac motor drive test. Using the model, energy and cost-effectiveness is analyzed and discussed.**

***Index Terms*—Mobile refrigeration unit (MRU), hybrid power systems, electric drives, lithium-ion batteries, average modeling**

I. Introduction

The development of hybrid technologies helps to reduce emissions and increase fuel economy in vehicles. In heavy trucks, hybridization can improve emissions and reduce energy consumption issues, particularly when these vehicles stay at idle for extended intervals. Many delivery trucks are equipped with mobile refrigeration units (MRUs) powered by auxiliary diesel engines. An MRU is a refrigeration system controlling the temperature in a truck shipping container, as shown in Figure 1. MRUs are used for temperature sensitive products, and the trucks can operate under a wide variety of driving conditions, including high-speed limited-access highways or low-speed local streets, hot or cold ambient temperatures, and possibly long times on station for loading and unloading [1-2]. An airborne toxic and control measure (ATCM) regulation has been proposed for MRU diesel engines to reduce particulate matter emissions by 95% and nitrogen oxides by 65% between 2004 and 2014 [3]. Converting an MRU to an ac motor driven system is possible although it requires extra hardware and labor cost. The main truck engine and other power sources such as batteries, through power electronic conversion, may be able to produce a more efficient system than a fully self-contained MRU. This requires investigation through modeling and simulation work.

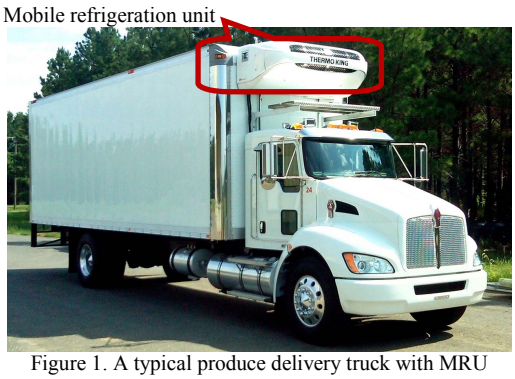

Figure 1. A typical produce delivery truck with MRU
Source: matrco.com

II. Hybrid Power System for MRU

A hybrid power system must provide consistent power for the thermal system whether the truck is mobile or not. Figure 2 shows the proposed hybrid system: a truck main engine shaft drives an ac generator feeding a rectifier with a stabilized output dc bus; then a dc-ac inverter connected to an ac induction machine drives the compressor; and the battery is in parallel and connects at the dc bus, possibly through a separate dc-dc converter. Grid plug-in could be available in place of the generator. A visual system layout is shown in Figure 3. The goal of the hybrid system model is to analyze long-term system and component response for practicality, hardware limitations, efficiency, and fuel cost. It is most important to observe the power and efficiency in each subsystem.

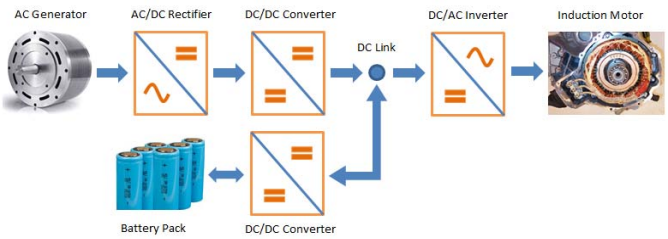

Figure 2. Hybrid power system structure in the simulation model

This work was supported in part by Thermo King, a division of Ingersoll-Rand, and by the Grainger Center for Electric Machinery and Electromechanics at the University of Illinois at Urbana-Champaign.

Yue Cao is with the Department of Electrical and Computer Engineering, University of Illinois, Urbana, IL 61801, USA (email: yuecao2@illinois.edu).

Philip. T. Krein is with the Department of Electrical and Computer Engineering, University of Illinois, Urbana, IL 61801, USA (email: krein@illinois.edu).

978-1-4799-0148-7/13/$31.00 ©2013 IEEE

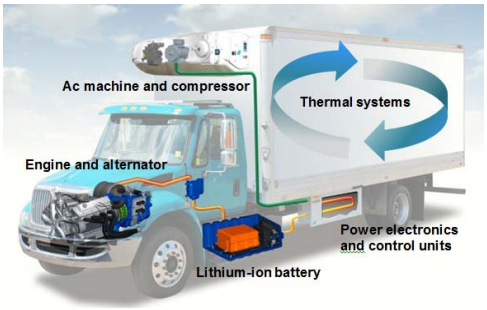

Figure 3. Physical layout of MRU major components, edited from [4] Courtesy of Thermo King Corporation, used by permission

III. Average Modeling Approach

A previous paper [5] compares averaging and detailed-dynamics modeling approaches for MRU applications. The study shows that the average model tolerates sampling times up to 0.1 s to accommodate different thermal or other electrical interfacing requirements, and the model simulates at least 10 times faster than what happens in real time. On the other hand, the detailed-dynamic model, including device switching and machine transients, has a maximum sampling time of 5 µs, and the model operates too slowly to be useful for a long-term efficiency and cost study as described in the goal.

For the average modeling approach suggested by [5], it seeks to model energy flows and power balances, including power losses in each subsystem (motor, converter, battery, etc.). The ac generator is modeled as a three-phase permanent magnet synchronous machine (PMSM) with continuous output rating of 17.3 kW. The ac motor that drives the compressor is modeled as a three-phase 12 HP 460 V 60 Hz induction machine (IM). The IM and PMSM models employ conventional per-phase steady-state equivalent circuits as shown in Figures 4 and 5 [6]. Machine mechanical losses must also be included. These can be inferred from machine data sheets and basic tests. Since the ac generator is coupled to the drive engine, its operating speed is linked to a dynamic vehicle drive cycle, and ranges from 1750 to 5000 RPM. For simulation studies reported here, drive cycle data were obtained from an industry study that recorded typical truck driving conditions [7]. A proposed daily drive cycle is depicted in Figure 6. The cycle is 10-hour (36,000 s) long and includes truck running and idling intervals.

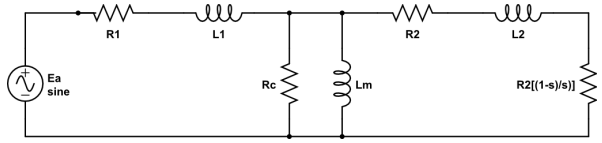

Figure 4. IM per-phase equivalent steady state circuit

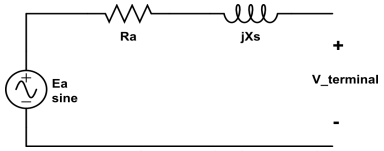

Figure 5 PMSM per-phase equivalent steady state circuit

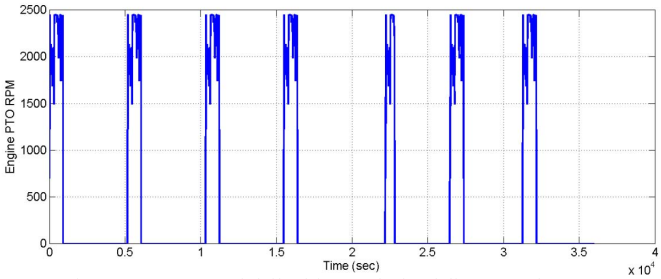

Figure 6. A proposed daily drive cycle for delivery trucks [7]

The rectifier, inverter, and any dc-dc converters are power electronic elements with switching losses and conduction losses in the IGBTs. These losses are modeled based on equivalent steady state conditions and estimated as [8]

$$P_{cond} = \frac{2\sqrt{2}I_{rms}V_{on}}{\pi} + I_{rms}^2 R_{ds} \quad (1)$$

and

$$P_{switch} = \frac{2\sqrt{2}I_{rms}V_{bus}}{\pi} f_{switch} \frac{t_{on}+t_{off}}{2} \quad (2)$$

The conduction loss can be modeled by means of an ideal switch in series with a forward voltage drop (V_{on}) and a series resistor (R_{ds}). In the switching loss calculation, f_{switch} is the inverter switching frequency. Times t_{on} and t_{off} are the IGBT switching rise and fall delay times, respectively, which are found in device datasheets. V_{bus} is the main dc bus voltage.

A scalar volts-per-hertz (V/f) control is implemented in the IM drive. The IM and PMSM are controlled to respond robustly to a wide range of torque and speed commands from the thermal system, and to engine dynamics associated with the vehicle driving cycle.

IV. Improved Battery Simulation

The battery model is based on the circuit in Figure 7 [9]. The second, minute, and hour based resistors and capacitors predict battery cell dynamics in each of the corresponding time frames. The battery terminal voltage is then calculated as

$$V_t = V_{oc} - I_c\left(R_{series} + R_{ts} \,\|\, \frac{1}{sC_{ts}} + R_{tm} \,\|\, \frac{1}{sC_{tm}} + R_{th} \,\|\, \frac{1}{sC_{th}}\right) \quad (3)$$

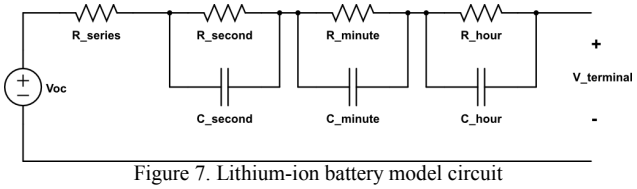

Figure 7. Lithium-ion battery model circuit

The voltage source, resistors, and capacitors depend non-linearly on the battery state of charge (SOC). In [9], V, C, and R values are modeled as sixth-order polynomials of SOC. Upon simulation using the parameters from [10], some polynomial curves can become negative, which creates instability in a system simulation (Figure 8). To remedy this, a logarithmic interpolation equation

$$\ln(V,C,R) = a_0 + a_1 \ln(SOC) + \ldots + a_6 \ln^6(SOC) = \sum_{k=0}^{6} a_k \ln^k(SOC) \quad (4)$$

is proposed. When this is used with real battery characteristics, the coefficient of determination (R^2) is a minimum of 0.8. One

fitting curve is also plotted in Figure 8 to compare with the original curve. The new method produces more accurate *V*, *C*, *R* values and models the battery more robustly. The coefficients of (4) are listed in Table 1. The labels (C) and (D) indicate coefficients for charging and discharging conditions. Single-cell data were extracted from measurements of Panasonic CGR18650A 3.7 V, 2.2 A-h Li-ion batteries [10].

The SOC is modeled based on

$$SOC(t) = SOC_{initial} + \int_0^t f_1[i_{charge}(t)] \times i_{charge}(t)dt + \int_0^t f_2[i_{discharge}(t)] \times i_{discharge}(t)dt \quad (5)$$

where the initial SOC is constant and defined prior to simulation, *i(t)* is the instantaneous discharging or charging current, and *f* is a function of that current and modeled as a 1-D lookup table. The relationships between *f* and *i* are given in Tables 2 and 3 for the charging and discharging [10].

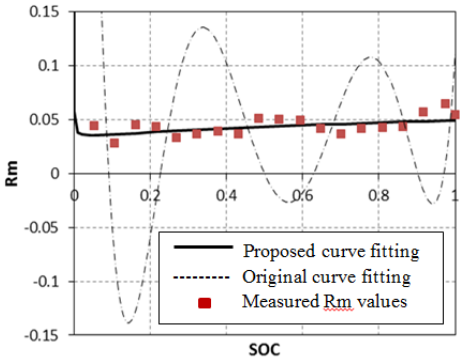

Figure 8. Proposed and original [10] curve fits for R_min constant

Table 1. Coefficients for functions used in Figure 6

	a0	a1	a2	a3	a4	a5	a6
Voc	1.4222	0.2214	0.1829	0.0745	0.0145	0.0014	5×10^{-5}
Rseries (D)	-2.9384	-0.2328	-0.2109	-0.1294	-0.0302	0	0
R_s (D)	-3.4883	-1.2434	-0.5619	0.0044	0.0348	0	0
C_s (D)	-0.146	0.3731	1.6511	1.0513	0.1918	0	0
R_m (D)	-3.1892	-0.0486	1.4851	6.1491	7.0124	3.1645	0.4997
C_m (D)	6.9413	-6.5951	-29.577	-56.356	-46.582	-16.991	-2.2588
Rseries (C)	-2.8108	0.6011	0.8951	0.436	0.07	0	0
R_s (C)	-3.5637	0.0016	3.4633	4.6412	2.2718	0.425	0.0188
C_s (C)	-0.2737	-3.4945	-14.705	-21.767	-14.113	-4.1803	-0.4632
R_m (C)	-2.8744	1.1014	1.1243	0.266	-0.1345	-0.046	0
C_m (C)	6.9622	-0.447	2.896	4.5575	2.2427	0.3544	0
R_h	-5.6352	5.1517	12.006	6.1973	0	0	0
C_h	14.622	-6.2451	-19.818	-11.446	0	0	0

Table 2. *f* and *i* relationship for the charging state

i (charge)	0	0.0838	0.4386	1.0988	2.202
f(i)	1.34×10^{-4}	1.3259×10^{-4}	1.2581×10^{-4}	1.2391×10^{-4}	1.2192×10^{-4}

Table 3. *f* and *i* relationship for the discharging state

i (discharge)	0	0.0808	0.4389	1.0886	2.1603
f(i)	-1.4×10^{-4}	-1.3751×10^{-4}	-1.2727×10^{-4}	-1.3222×10^{-4}	-1.3928×10^{-4}

V. Simulation Study

A comprehensive simulation must be run for the integrated thermal-electrical system. It is important to evaluate performance under real-life scenarios, which include the vehicle drive cycle, dynamic thermal loading demand based on the desired truck container temperature and ambient temperature, door open and close events, connection to grid power, etc. The energy flow is developed in reverse order: based on thermal requirements, the compressor has known speed and torque requirements. These in turn are supplied by the induction machine, and to this machine by the inverter. The inverter draws power from the generator or the batteries. Generator operation is linked to engine RPM during the vehicle drive cycle, sitting idle at minimum speed when the vehicle stops.

To demonstrate the capabilities of the average model, a system simulation from 20,000 s to 29,000 s, corresponding to 1:00 PM to 3:30 PM during a typical day's delivery schedule, is prepared. The motor operates when there is demand from the thermal system. The battery is charged, if below a preset SOC value, when the generator runs, and it is discharged when the motor is on while the truck is not moving. The truck delivers products under a proposed ambient temperature profile, around 34 °C. The products require a temperature maintained between -30 °C and -25 °C. Figures 9-11 show the power levels at each component in the hybrid power system. Notice that the time units reflect an interval nearly three hours long.

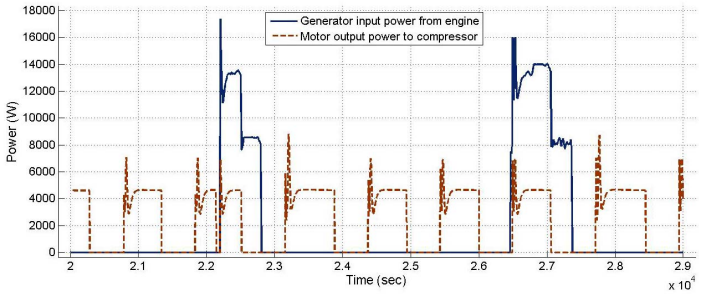

Figure 9. Machines (generator, motor) power levels

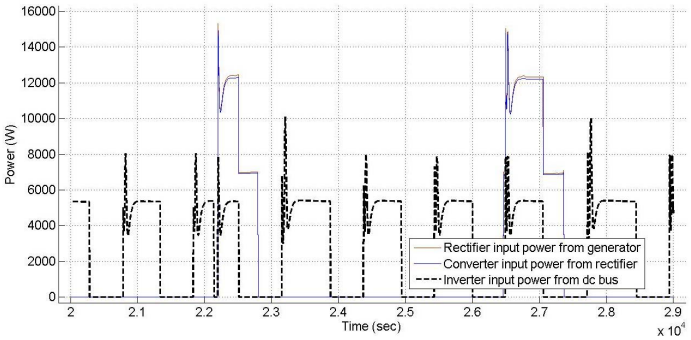

Figure 10. Power electronics (rectifier, converter, inverter) power levels

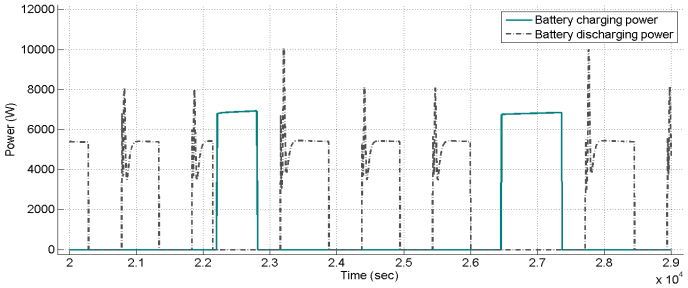

Figure 11. Battery charging and discharging power levels

Given the power levels obtained from the above simulation, efficiency curves can be defined and plotted. In Figure 12, the engine power supply efficiency is calculated as the ratio of power to the compressor and power into the generator excluding the power used for battery charging. In Figure 13, battery power supply efficiency is the ratio of power to the compressor and power out of the battery pack.

The battery's SOC and terminal voltage are simulated in Figures 14 and 15, respectively. With all the above power system and thermal system components integrated properly, a desired temperature profile is achieved as shown in Figure 16.

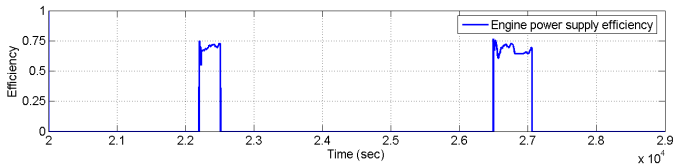

Figure 12. Engine power supply efficiency

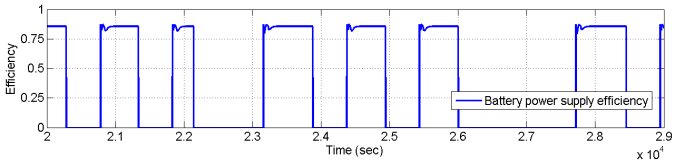

Figure 13. Battery power supply efficiency

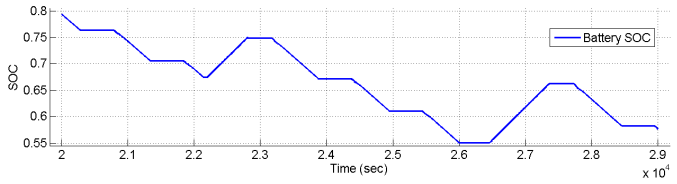

Figure 14. Battery SOC change

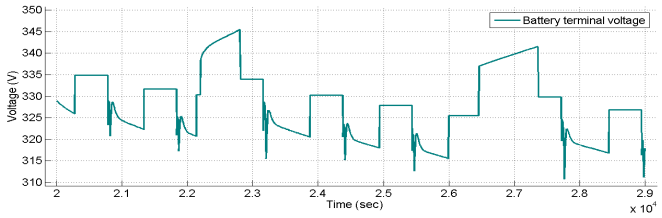

Figure 15. Terminal voltage of the battery pack

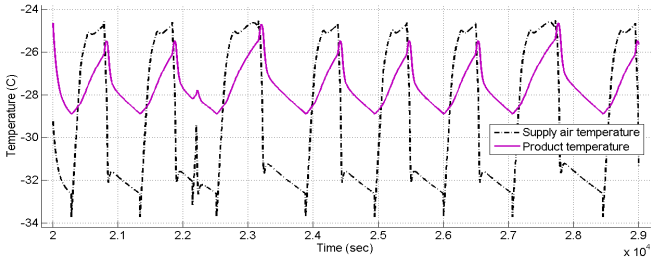

Figure 16. Temperature change in the container

VI. Experimental Validation

Tests of the generator and the ac-dc rectifier were conducted separately [11]. A three-phase PMSM, the one modeled in Simulink, was used in the experimental tests. This device was used previously for an electric air conditioning unit in a city bus. Different loads were applied for each of various speed settings, and the corresponding power losses and efficiencies were obtained through direct measurement, as shown in Figure 17. The simulated power losses and efficiencies are plotted in dashed lines; and solid lines show the actual data. It can be observed that the simulation power loss prediction is within 6% deviation from the actual data over most of the operating range. The simulated and measured efficiencies are within 1% of each other.

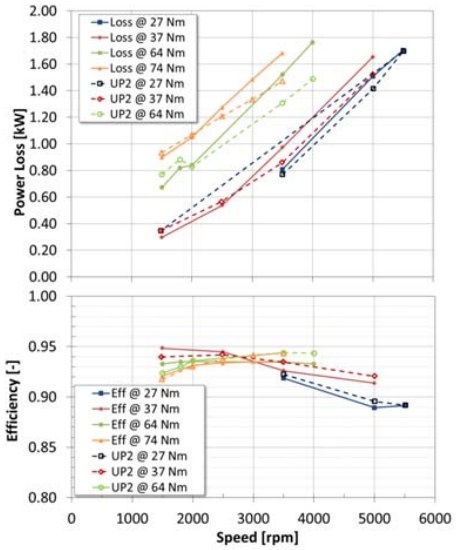

Figure 17. PMSM power loss and efficiency versus speed at different loads from [11], courtesy of Thermo King Corporation, used by permission

To validate the improved battery modeling approach, test data for the *R* and *C* constants and open circuit voltage in Figure 7 were obtained and plotted against the model simulation. The test data are available from [10]. Figure 18 is the battery cell open circuit terminal voltage (simulated and measured) as a function of SOC.

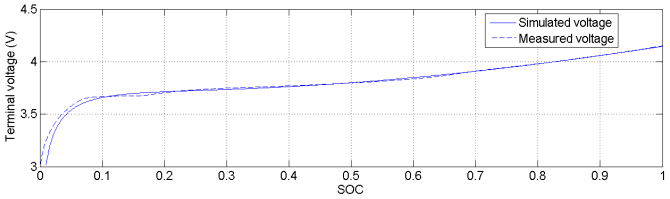

Figure 18. Measured battery terminal voltage compared to simulated data

A hardware test bed for the variable frequency ac motor drive, including the dc-ac inverter and the motor is shown in Figure 19. The system operates at about 1/6 scale compared to the vehicle system. A three-phase 230 V 2 HP 4-pole IM was chosen, and a modular dc-ac inverter was used. The control box of the inverter is based on a TI-2812 DSP and commanded by MATLAB/Simulink [12]. The inverter was controlled to vary frequencies (50 Hz, 60 Hz, and 70 Hz) and voltages based on the V/f ratio. For each frequency, different loads from a dynamometer were applied, and corresponding motor speed, inverter input and motor output power, and drive efficiency were obtained. Parameters of this 2 HP IM were used for a separate simulation run. Measured efficiency and simulated efficiency are plotted in Figure 20. The two efficiency curves are within 3% of each other. Generally, the average model efficiency is somewhat higher since it does not include harmonics losses as a real system does [5].

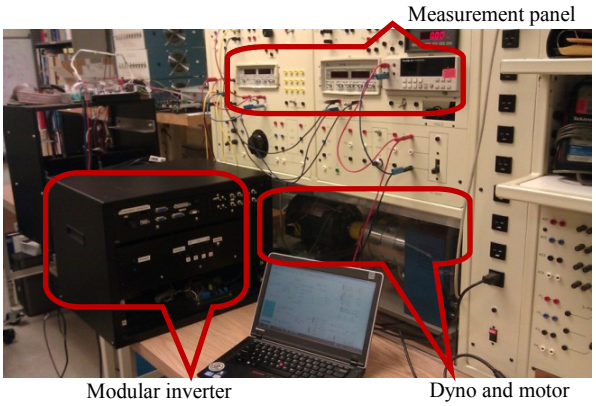

Figure 19. Experiment setup for the power system testing

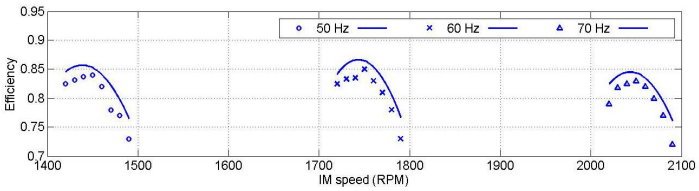

Figure 20. Measured (dots) and simulated (lines) motor drive efficiency

VII. Cost Effectiveness and Limitation

The simulated scenario in Section V is used and extended to 0 s to 36,000 s to represent a whole day. The battery pack is pre-charged from the grid before deliveries, and it is charged by the generator as needed during the deliveries. A 6 kWh battery pack is chosen such that it is depleted by the end of the day under this relatively severe test scenario. The battery is then recharged from the grid overnight. Assuming 40%, 25%, and 90% efficiency for the medium-duty truck main engine, the light-duty compressor engine in the conventional system, and the battery charger, respectively [13], daily hybrid and conventional MRU consumed energy, through integration of power, can be calculated and summarized in Table 4. The table also includes the total cost per day, assuming 135.6 MJ/gal in the diesel fuel [13] at $4.00/gal and $0.10/kWh for electricity [14]. The same analysis, also presented in Table 4, is performed for a plug-in only option with no battery and for a 50-50 combined plug-in and battery option with a reduced-size battery pack.

Table 4. Energy and cost comparison among different configurations

	Hybrid	Conventional	Plug-in only	50% Plug-in and 50% battery
Diesel fuel (gal)	1.75	2.45	0.35	0.80
Electricity (kWh)	6.67	0	24.5	15.6
Total energy (MJ)	261.87	332.76	135.12	165.2
Total cost ($)	7.67	9.80	3.85	4.76

Both the hybrid and plug-in enabled power systems outperform the conventional power system, but hybrid and plug-in options have higher initial costs from power electronics, battery, and charging stations. Figure 21 illustrates the total cost of each system configuration during the first eight years, assuming that the truck operates six days a week, and that the diesel engine for the conventional system requires regular oil/filter and air filter changes. The figure shows that after three years the options with plug-in outperform the conventional system, and after four years, the hybrid option also becomes advantageous. Note that a large portion of plug-in fixed costs comes from chargers or charging stations. It may take less time for break-even if such cost is not directly out of a customer's pocket or if a "charging station" is just an electric outlet.

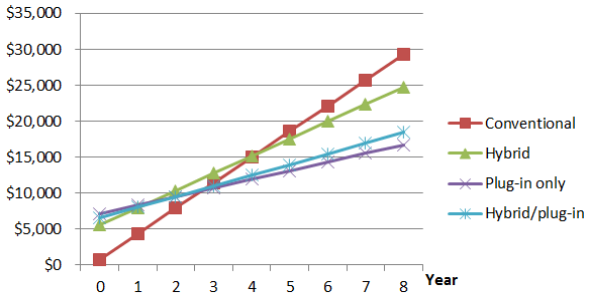

Figure 21. Comparison of total costs over eight years

The analysis above is based on the operating conditions described in Section V. Other operating conditions will yield different energy and cost savings results. For example, if the truck makes mostly inter-city deliveries, the plug-in options are less attractive because there are few stops. In this case, the hybrid power system seems the best option to comply with environmental regulations. With other scenarios considered, a comprehensive energy and cost savings analysis is required for the future in order to target different MRU applications.

The average model has a few limitations and considerations. 1) The model runs fast by trading off fidelity. The model is not intended for use in detailed hardware design, and it is not helpful for observing system behavior in a short time interval

especially during vehicle acceleration or deceleration. 2) Various drive cycles and loading profiles are appropriate for a most thorough system analysis. The scenario described in this paper keeps produce frozen on a hot summer day for a local delivery truck. Another scenario of long-distance highway transport will have a different result. An MRU may also be required to maintain fresh produce above 0 °C when the outside temperature is -20 °C. In this case, the MRU must supply warm air, and depending on the heating unit, the power system may or may not be modified. 3) The hybrid model presented is based on a parallel hybrid topology. Series hybrid or other topologies may be equivalently functional. One alternative directly couples the PMSM with the IM. The idea is feasible because the PMSM itself acts like a volts-per-hertz control due to the linear relationships between V, f and rotor speed. However, further study may be required, as the PMSM has a wide range of outputs.

VIII. Conclusion

A hybrid power system for mobile refrigeration applications has been designed, modeled, and tested. The proposed average model, interfaced with the thermal system model, has been validated by comprehensive simulation and experimental work. The average model with improved battery formulation enhances accuracy and robustness for battery subsystem simulation. In addition to fast simulation, the model is flexible and can run at desired times, power levels, and drive cycles. The average model has been applied as part of a complete thermal-electric system simulation and serves as a basis for future energy storage selection and hybrid system optimization studies.

The electrification of an MRU is a recent topic in industry and has potential, including 1) advanced existing or novel motor drive control techniques for highly efficient and precise internal loading requirement, 2) grid interfacing issues regarding government policy, smart grid, pricing, or system reliability, etc., and 3) modeling strategy, such as the piece-wise linear method suggested by [15], which is capable of reaching the simulation speed goal but also providing more detail.

References

[1] C. V. Kulkarni, "Modeling and the performance analysis of transportation refrigeration units with alternate power systems," Ph.D. dissertation, Mechanical and Aeronautical Engineering, Univ. of California, Davis, CA, 2007.

[2] M. Duvall, et al., "Transportation refrigeration equipment: cost-effective emissions reduction," EPRI, Palo Alto, CA, Rep. 1008774, 2004.

[3] California Air Resources Board, "Airbourne toxic control measure for in-use diesel fueled transportation refrigeration units (TRU) and TRU generation units, and facilities where TRUs operate," CARB, 2003.

[4] B. Mohs, et al., "Truck hybridization architecture and control study – Thermo King and Ingersoll Rand," unpublished, 2011.

[5] Y. Cao and P. T. Krein, "Average and detailed modeling approaches emphasizing subsystems in a hybrid mobile refrigeration," in *Proc. IEEE International Electric Machines and Drives Conf.*, 2013.

[6] A. E. Fitzgerald, C. Kingsley, and S. D. Umans, *Electric Machinery*, 6th ed. NY: McGraw Hill, 2003, pp. 306-348.

[7] R. A. Jackey, "A simple, effective lead-acid battery modeling process for electrical system component selection," The Mathworks Inc., Novi, MI, Rep. 2007-01-0778, 2007.

[8] P. T. Krein, *Elements of Power Electronics*. New York: Oxford University Press, 1998, pp. 451-530.

[9] R. C. Kroeze and P. T. Krein, "Electrical battery model for use in dynamic electric vehicle simulations," in *Proc. IEEE Power Electronics Specialists Conf.*, 2008, pp. 1336-1342.

[10] R. C. Kroeze, "Electrical battery model for use in dynamic electric vehicle simulations," M.S. thesis, Electrical and Computer Engineering, Univ. of Illinois, Urbana, IL, 2008.

[11] P. Kadanik, et al., "Transport hybridization study sponsor update – Thermo King and Ingersoll Rand," unpublished, 2012.

[12] J. Kimball, et al., "Modular inverter for advanced control applications," Grainger Center for Electric Machinery and Electromechanics, Urbana, IL, CEME-TR-2006-01, 2006.

[13] National Petroleum Council, "Heavy-duty engines & vehicles analysis – advancing technology for America's transportation future," NPC, Washington D.C., Rep. 2012950513, 2012.

[14] Bureau of Labor Statistics, "Average energy prices in the Chicago area," BLS, Midwest Information Office, 13-233-CHI, 2013.

[15] J. H. Allmeling and W. P. Hammer, "PLECS - piece-wise linear electrical circuit simulation for Simulink," in *Proc. IEEE International Conference on Power Electronics and Drive Systems*, 1999, pp. 355–360.